Microscopy, 2022, **71(3)**, 169–174
DOI: https://doi.org/10.1093/jmicro/dfac009
Advance Access Publication Date: 17 February 2022
Article

MICROSCOPY

Analytical technique for self-absorption structure of iron *L*-emission spectra obtained by soft X-ray emission spectrometer

Takaomi D. Yokoyama[1,*], Hideyuki Takahashi[1], Shogo Koshiya[1], Takanori Murano[1] and Masami Terauchi[2]

[1]SA Research and Development Department, JEOL Ltd., 3-1-2 Musashino, Akishima, Tokyo 196-8558, Japan
[2]Institute of Multidisciplinary Research for Advanced Materials, Tohoku University, Sendai 980-8557, Japan
*To whom correspondence should be addressed. E-mail: takayoko@jeol.co.jp

Abstract

The method deriving the *L* self-absorption spectrum from *Lα,β* emission spectra obtained at different accelerating voltages has been optimized for analyzing the chemical state of Fe in solid materials. Fe *Lα,β* emission spectra obtained are fitted using Pseudo-Voigt functions and normalized by the integrated intensity of each Fe *Ll* line, which is not affected by $L_{2,3}$ absorption edge. The self-absorption spectrum is calculated by dividing the normalized intensity profile collected at low accelerating voltage by that collected at a higher accelerating voltage. The obtained profile is referred to as soft X-ray self-absorption structure (SX-SAS). This method is applied to six Fe-based materials (Fe metal, FeO, Fe_3O_4, Fe_2O_3, FeS and FeS_2) to observe different chemical states of Fe in those materials. By comparing the self-absorption spectra of iron oxides, one can observe the L_3 absorption peak structure shows a shift to the higher energy side as ferric (3+) Fe increases with respect to ferrous (+2) Fe. The intensity profiles of self-absorption spectra of metallic Fe and FeS_2 shows shoulder structures between the L_3 and L_2 absorption peaks, which were not observed in spectra of Fe oxides. These results indicate that the SX-SAS technique is useful to examine X-ray absorption structure as a means to understand the chemical states of transition metal elements.

Key words: electron probe microanalyzer, soft X-ray emission spectrometer, self-absorption, X-ray absorption structure, chemical state analysis, Fe

Introduction

Chemical state analysis using spectral shapes of characteristic X-ray emissions is a widely recognized technique and the method has been conducted mainly using wavelength dispersive (WD) spectrometry on electron probe microanalyzer (EPMA). Recently, a soft X-ray emission spectroscopy (SXES) instrument was developed as a new type of WD spectrometer that can be attached to either an EPMA or scanning electron microscopes (SEM) [1,2]. X-ray dispersion of the SXES instrument uses fixed varied-line-spacing diffraction gratings, which were designed to focus X-rays onto a CCD detector plane in a certain energy range [3–5]. The SXES instrument is capable of a parallel detection of multiple characteristic X-ray spectra with a high signal-to-noise ratio (S/N). Current spectrometers have a detectable energy range from 50 to 210 eV and from 100 to 2300 eV.

The *Lα,β* emission lines of first-transition metal elements are originating from the electronic transitions from the valence bands to the inner $L_{2,3}$-shell ($2p$) levels. These transition energies contain information on the energy distribution of $3d$ and show chemical shift of the $2p$ inner-shell levels. Thus, the analyses of *L*-emission spectra of first-transition metal elements have been applied for chemical state analyses and quantitative analyses. For example, the flank method is available for the measurement of Fe valence number in the silicate (mainly garnet-type) minerals using EPMA [6–8]. This method evaluates the differences between the spectra of divalent and trivalent Fe-bearing minerals by comparing *Lβ*/*Lα* intensity ratios, which were measured at fixed *Lβ* and *Lα* wavelength positions.

On the other hand, it has been pointed out in previous studies that the spectral shapes and the peak energies of *L*-emission spectra from the same chemical species containing several transition metal elements can vary depending upon the accelerating voltage of the incident electron beam [7,9,10]. Figure 1a shows Fe *Lα,β* emission spectra of FeO acquired at various accelerating voltages using an SXES instrument attached to an EPMA. The peak positions of *Lα* shows shifts depending on the accelerating voltages. This apparent peak shift is due to the self-absorption effect for *Lα,β* emission because *Lα,β* emission energy is almost overlapped with $L_{2,3}$ absorption edge energy, and an incident electron beam of a higher accelerating voltage causes an X-ray emission source at a deeper region form the specimen surface than that of a lower accelerating voltage [7,9,10]. These self-absorption effects can be visualized as self-absorption spectra by calculating logarithmic intensity ratios of X-ray emission spectra obtained at various accelerating voltages as shown in Fig. 1b [11].

Received 16 November 2021; Revised 2 February 2022; Editorial Decision 13 February 2022; Accepted 17 February 2022

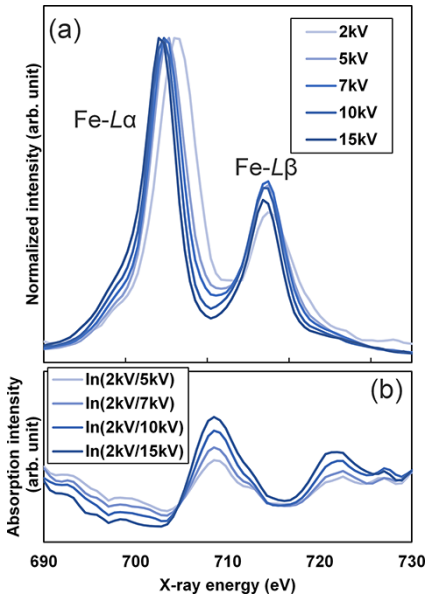

Fig. 1. (a) Fe *L*-emission spectra obtained at accelerating voltages of 2, 5, 7, 10 and 15 kV. (b) Calculated self-absorption spectra of FeO.

Previous studies attributed the peak positions that appeared in the self-absorption spectra correspond to the *L* absorption edges [7,9–11].

Self-absorption spectra derived from X-ray emission measurement using EPMA have been reported as a direct method to indicate the influence of self-absorption effects that interfere with the assign of the chemical state of materials. The present systematic study of the use of self-absorption spectra themselves for chemical state analysis represents a new analytical technique. Conventional wavelength dispersive spectroscopy (WDS) requires serial detection of X-rays and scanning by simultaneous mechanical movement of the crystal and detector, which increases the counting time. In contrast to the WDS, the parallel detection system of SXES is an ideal solution for the collection of X-ray spectra, which offers the ability to collect an X-ray spectrum in relatively short acquisition time and offers an easier approach to collecting spectra at varying accelerating voltages to derive a self-absorption spectrum. Another significant advantage of the fixed grating spectrometer is that it provides a high reproducibility of measurement of X-ray energy in multiple measurements with varying conditions compared to the traditional WD spectrometry.

We investigate the application of obtaining self-absorption spectra from a series of Fe-based materials using an SXES instrument attached to an EPMA. The chemical shifts and changes of intensity profile of derived self-absorption spectra are discussed.

Experimental and energy calibration

Six polished solid samples of Fe-based materials (Fe metal, FeO, Fe_3O_4, Fe_2O_3, FeS and FeS_2) were prepared for obtaining X-ray *L*-emission spectra at a series of accelerating voltages chosen to provide a range of self-absorption effect. The SXES instrument used in this study was an SXES-ER using a JS2000 grating (dispersive range: 230–2300 eV) attached to a field emission EPMA, JEOL JXA-iHP200F. Fe *L*-emission spectra were acquired at accelerating voltages of 2, 5, 7, 10 and 15 kV to measure differences in the self-absorption spectra under each condition. Probe current was from 10 to 50 nA. Probe diameter was 20 μm. The acquisition time for each spectrum at each accelerating voltage was 5 min.

Fe *L*-emission is composed of four components, *L*α, *L*β, *L*l and *L*η. *L*α,β emission energy of about 710 eV is almost the same energy range with that of $L_{2,3}$ absorption edge. Thus, *L*α and *L*β emission is affected by $L_{2,3}$ absorption edge, better known as the self-absorption effect. This effect causes a change in peak shape depending on accelerating voltages. By comparison, *L*l,η emission energy of about 615 eV is lower than the $L_{2,3}$ absorption edge and consequently unaffected. Figure 2 shows Fe *L*l and *L*α emission spectra of metallic iron obtained at various accelerating voltages. A fitting curve for the spectrum obtained at 15 kV is also shown. Each intensity was normalized by each peak height of intensity. It is seen that the *L*l peak shape is not changed by accelerating voltages, confirming no absorption effect of $L_{2,3}$ edge (Fig. 2a). In contrast, *L*α emission peak profile changes depending on the accelerating voltage due to the absorption effect of $L_{2,3}$ edge (Fig. 2b). The energy calibration of the spectrometer was carried out by

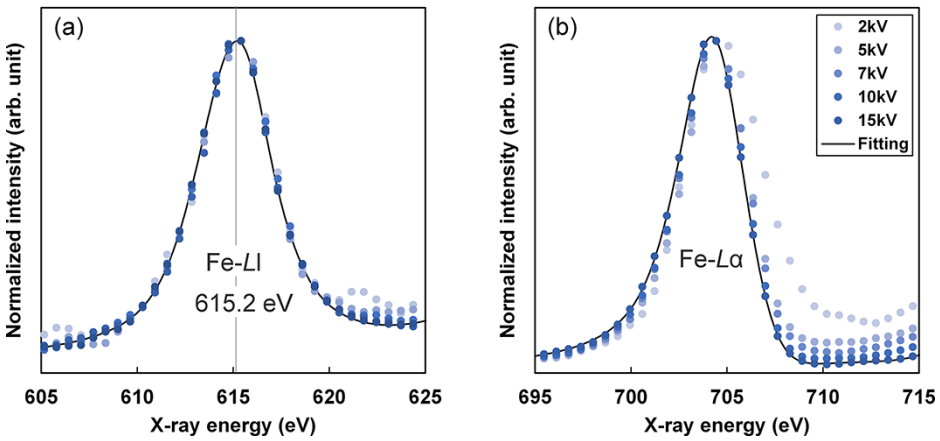

Fig. 2. (a) Fe *L*l line and (b) Fe *L*α line spectra of metallic iron obtained at 2, 5, 7, 10 and 15 kV. Spectral intensities are normalized in each spectrum. Fitting curves of Fe *L*l and *L*α peaks obtained for 15 kV.

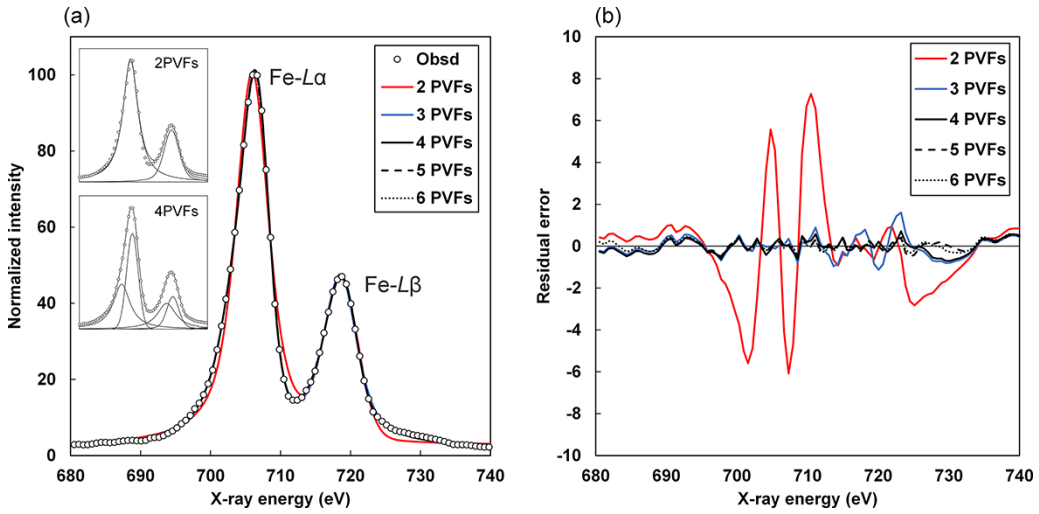

Fig. 3. (a) Fe $L\alpha,\beta$ spectrum of Fe_2O_3 at 7 kV and fitted curves using multi PVFs. (b) Residual errors between the experimental spectra and fitting curves.

fixing the Fe Ll emission peak energy of metallic iron to be 615.2 eV [12].

Results and discussion

Fitting calculation

The intensity profile of $L\alpha$ and $L\beta$ emission peaks reflect the partial density of states of valence bands reflecting the dipole selection rule. The intensity profiles reflect the chemical bonding states of materials examined. The intensity profiles are not necessarily symmetric [10]. These peak positions are also affected by a chemical shift of $L_{2,3}$ inner-shell levels, which depend on the valence of the Fe atom [13]. An additional effect leading to a change of $L\alpha$ and $L\beta$ intensity profile is the self-absorption effect due to a presence of $L_{2,3}$ absorption edge in the same energy region.

Prior to calculating the experimental intensity profiles, each spectrum intensity was normalized so that the maximum signal intensity was set to 100, enabling the residual in the fitting evaluations to be comparable across each spectrum. Then, the least square fitting calculations were performed for $L\alpha,\beta$ intensity profile using multiple Pseudo-Voigt functions (PVFs) [14]. The background intensity was fitted using a linear function. In the fitting calculation, the noise level of the self-absorption spectra finally obtained changes depending upon the fitting algorithm employed. The relational between the measured intensity and the fitting functions is expressed as

$$I_O = f_1(E) + f_2(E) + \cdots f_n(E) + B(E) + \varepsilon,$$

where f_n(E) are PVFs, B(E) is a linear function for the background intensity, and ε is the residual error between the measured value and the reproduced value by fitting.

Figure 3a shows $L\alpha$ and $L\beta$ peaks of Fe_2O_3 obtained at an accelerating voltage of 7 kV. Fitted curves by using different numbers of PVFs are also shown, and all fitting curves are plotted by calculating the relative intensity per 0.1 eV from the fitting function. When the $L\alpha$ and $L\beta$ region is fitted using two PVFs, the intensity profile cannot be reproduced well seen as a large residual error ε in Fig. 3b. By adding a further PVF to the $L\alpha$ region (three PVFs), the residual error is significantly reduced in the region. By adding another PVF to the $L\beta$ region (four PVFs), the residual errors around 720 eV are reduced as seen in Fig. 3b. The fittings using five and six PVFs did not show a further improvement compared with that of four PVFs. Thus, intensity profiles of $L\alpha,\beta$ peak are fitted by using four PVFs in the following analysis.

Extraction and comparison of Fe self-absorption spectra

SXES instrument used can detect Fe Ll, $L\eta$, $L\alpha$ and $L\beta$ spectra at the same time. Since the Fe Ll line is not affected by $L_{2,3}$ absorption edge, the spectral intensity I_L is normalized by the integrated peak intensity of Ll, I_{Ll} for comparing the self-absorption effect on $L\alpha,\beta$ intensity profile due to $L_{2,3}$ absorption (Fig. 4),

$$I_N = \frac{I_L}{I_{Ll}}.$$

I_N is the normalized intensity distribution. Self-absorption spectrum is displayed in the natural logarithm from a normalized intensity distribution I_{NL} obtained at a lower accelerating voltage divided by I_{NH} obtained at a higher accelerating voltage, $\ln(I_{NL}/I_{NH})$, should be taken [11]. In practical experiments as shown in Fig. 4, the intensity ratio of I_{NL}/I_{NH} in $L\alpha,\beta$ region ranges from 1 to 10. The $\ln(I_{NL}/I_{NH})$ could be approximated by I_{NL}/I_{NH}, which is simpler to evaluate. Self-absorption spectra (A) in this report are evaluated by the following manner,

$$A = \frac{I_{NL}}{I_{NH}}.$$

Spectral shapes and energy positions of self-absorption peaks

Figure 5 shows normalized Fe $L\alpha,\beta$ emission intensities of (a) FeO (Fe^{2+}) and (b) Fe_2O_3 (Fe^{3+}) obtained at accelerating voltages of 2, 5, 7, 10 and 15 kV. A clear shift of Fe $L\alpha$ peak to the lower-energy side occurs as the accelerating voltage increases for each material. Self-absorption spectra A of the materials are derived from intensity profiles I_{NL} of 2 kV divided by I_{NH} of 5, 7, 10 and 15 kV. The self-absorption spectra are shown

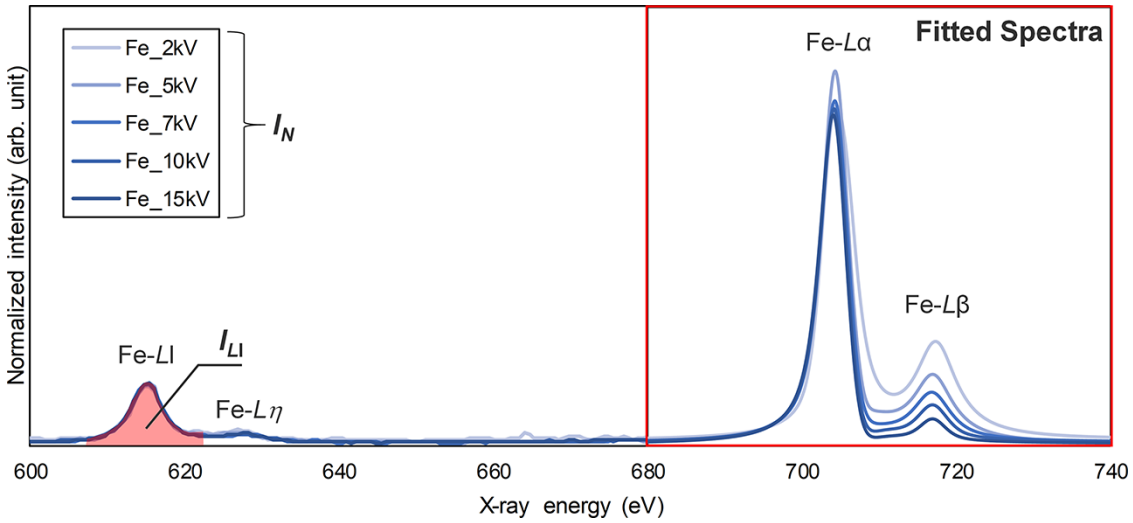

Fig. 4. Fe *L* spectra of *L*α, *L*β, *Ll* and *L*η normalized by integrated intensities of Fe *Ll* line.

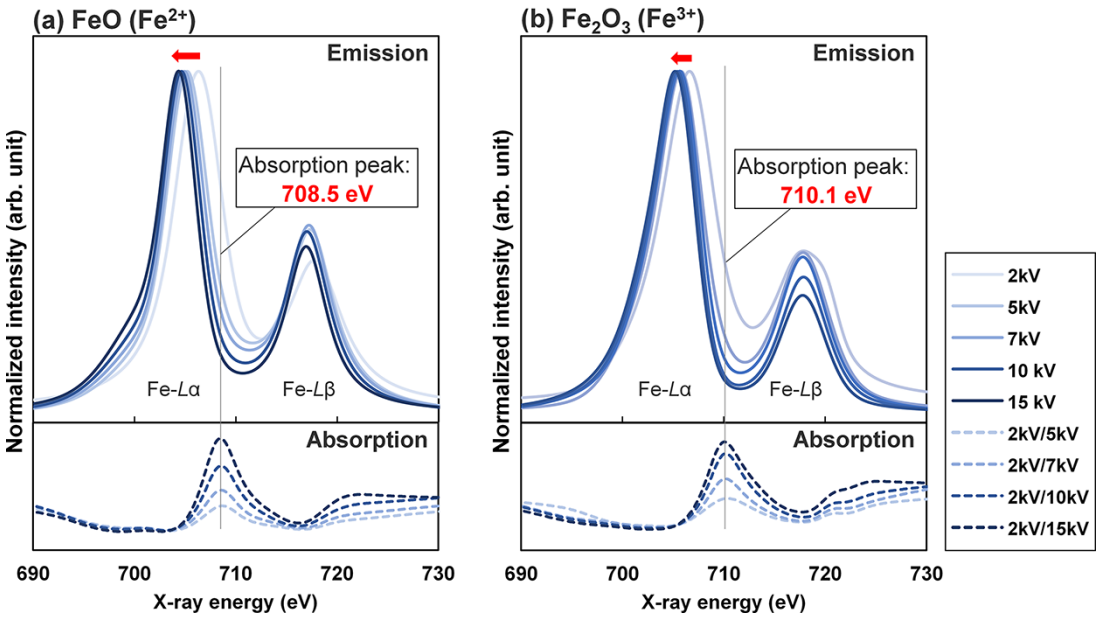

Fig. 5. Fe *L*-emission and obtained self-absorption spectra of (a) FeO (Fe^{2+}) and (b) Fe_2O_3 (Fe^{3+}). Although the emission peak position depends on the accelerating voltage due to self-absorption effect, absorption peak derived is not.

by dotted lines below the Fe *L*α,β emission intensity profiles of each material. It can be seen that the absorption peak position at about 710 eV is unchanged by the accelerating voltage. The fact that the absorption peak position is fixed enables this approach to be made. The self-absorption spectrum is referred to as the soft X-ray self-absorption structure (SX-SAS).

The absorption peaks at 708.5 eV for FeO and 710.1 eV for Fe_2O_3 should correspond to L_3 absorption peaks of the materials. A structure in 720–725 eV of each material should correspond to L_2 absorption peak structure. The higher L_3 absorption peak energy of Fe_2O_3 by 1.6 eV than that of FeO appears to be due to a chemical shift of Fe L_3-level resulting from the higher valence of Fe^{3+} in Fe_2O_3 compared to Fe^{2+} in FeO. A chemical shift of a core-level electron should result in a shift in both the self-absorption and the emission intensity. However, the *L*α shift with accelerating voltage of FeO is larger than that of Fe_2O_3 as indicated in Fig. 5 by lateral arrows. Thus, the difference is originated from a different intensity distribution of *L*α emission and L_3 absorption peaks and the energy separation, which are shown for different materials; see Fig. 5.

Figure 6 shows self-absorption spectra obtained for Fe metal, FeO, Fe_3O_4, Fe_2O_3, FeS and FeS_2. The peak structures at about 710 and 720 eV correspond to L_3 and L_2 absorption edges, respectively. The L_3 peaks of Fe oxides are systematically shifted to the high-energy side with an increase in the oxidation state of Fe from Fe^{2+} of FeO to Fe^{3+} of Fe_2O_3, and the L_3 peaks of sulfides of FeS (Fe^{2+}) and FeS_2 (Fe^{4+}) also show a similar shift to the high-energy side with a higher oxidation state. The systematic shifts of the L_3 absorption peak with the change in oxidation state have been reported by electron energy-loss spectroscopy (EELS) studies [15,16],

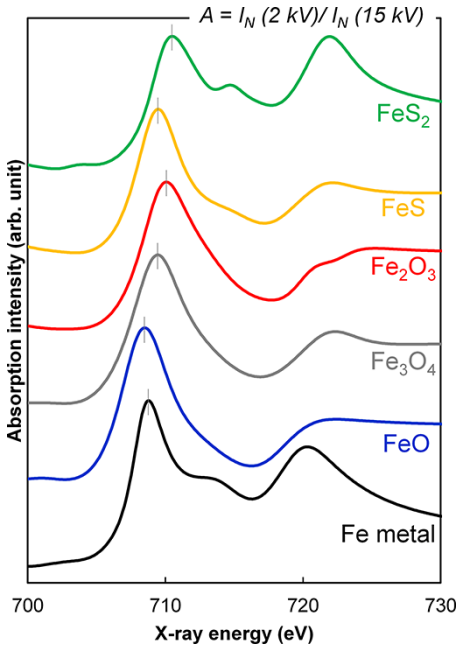

Fig. 6. Self-absorption spectra of Fe-based materials (metal, oxides and sulfides). Chemical shifts in different oxidation state of Fe were successfully observed.

and the SX-SAS results are consistent with these previous studies. The self-absorption spectra of metallic Fe and FeS_2 show additional shoulder structures at around 715 eV, which are consistent with EELS [17] and X-ray absorption fine structure (XAFS) experiments [18]. Although chemical shifts in different oxidation states of Fe were successfully observed by present SX-SAS method, more fine separated structures of energy states than Fig. 6 have been reported by EELS and XAFS experiments [16,19]. As the energy resolution of this method depends on the resolution of SXES, a further development of SXES spectrometer is necessary. Another factor that affects the energy resolution of this method, which is not taken into account in the present evaluation, is the spatial distribution of X-ray emission sources produced by the incident electron probe.

Concluding remarks

A systematic method to derive a Fe *L* self-absorption spectrum from experimental *L*-emission spectra, named SX-SAS, is presented. This method could also be done by using a conventional EPMA of serial detection in principle, except problems of reproducibility and an S/N of data. The parallel detection of a recent SXES instrument without a moving mechanism realizes a good signal-to-noise ratio in a shorter acquisition time. Fitting calculation using four PVFs was able to reproduce the $L\alpha$,β emission spectra with a small enough residual error for Fe-based materials. The self-absorption spectra of SX-SAS were evaluated by a simple division of I_{NL}/I_{NH}. The present energy resolution of SX-SAS is not enough compared with those of EELS and XANES, but chemical shifts in different charged states of Fe were successfully observed. Further application of this method by using a recent SXES system for 3*d*-transition metal elements is interesting, especially in Li-ion battery materials [20].

Acknowledgements

The authors would like to thank Dr. Terumi Ejima in Shinshu University, Dr. Yoshiaki Kon in Geological Survey of Japan, National Institute of Advanced Industrial Science and Technology, Dr. Kenichi Tsutsumi, Dr. Masahide Shima, Mr. Naoki Muraya in JEOL Ltd. and Dr. Calum Dickinson in JEOL (UK) Ltd. for helpful discussions and cooperation.

References

1. Takahashi H, Murano T, Asahina S, Terauchi M, Koike M, Imazono T, Koeda M, and Nagano T (2016) Development of soft X-ray emission spectrometer for EPMA/SEM and its application. *IOP Conf. Ser. Mater. Sci. Eng.* 109: 12017.
2. Terauchi M, Takahashi H, Takakura M, Murano T, and Koshiya S (2020) *Handbook of Soft X-ray Emission Spectra. Sixth edition*, (JEOL Ltd., Tokyo).
3. Terauchi M, Koike M, Fukushima K, and Kimura A (2010) Development of wavelength-dispersive soft X-ray emission spectrometers for transmission electron microscopes—an introduction of valence electron spectroscopy for transmission electron microscopy. *J. Electron Microsc.* 59: 251–261.
4. Terauchi M, Takahashi H, Honda N, Murano T, Koike M, Kawachi T, Imazono T, Koeda M, Nagano T, Sasai H, Oue Y, Yonezawa A, and Kuramoto S (2012) Ultrasoft-X-ray emission spectroscopy using a newly designed wavelength-dispersive spectrometer attached to a transmission electron microscope. *J. Electron Microsc.* 61: 1–8.
5. Terauchi M, Koshiya S, Satoh F, Takahashi H, Handa N, Murano T, Koike M, Imazono T, Koeda M, Nagano T, Sasai H, Oue Y, Yonezawa Z, and Kuramoto S (2014) Chemical state information of bulk specimens obtained by SEM-based soft-X-ray emission spectrometry. *Microsc. Microanal.* 20: 692–697.
6. Hoöfer H E, Brey G P, Schulz-Dobrick B, and Oberhaensli R (1994) The determination of the oxidation state of iron by the electron microprobe. *Eur. J. Mineral.* 6: 407–418.
7. Hoöfer H E and Brey G P (2007) The iron oxidation state of garnet by electron microprobe: its determination with the flank method combined with major-element analysis. *Am. Mineral.* 92: 873–885.
8. Borfecchia E (2012) Iron oxidation state in garnet from a subduction setting: a micro-XANES and electron microprobe ('flank method') comparative study. *J. Anal. At. Spectrom.* 27: 1725–1733.
9. Rémond G, Cilles C, Fialin M, Rouer O, Marinenko R, Myklebust R, and Newbury D (1996) Intensity measurement of wavelength dispersive X-ray emission bands: applications to the soft X-ray region. In: Benoit D, Bresse J-F, Van't dack L, Werner H, and Wernisch J (eds.), *Microbeam and Nanobeam Analysis, Microchimica Acta Supplement, Vol. 13*, pp 61–86 (Springer, Vienna).
10. Rémond G, Myklebust R, Fialin M, Nockolds C, Phillips M, and Roques-Carmes C (2002) Decomposition of wavelength dispersive X-ray spectra. *J. Res. Natl. Inst. Stand. Technol.* 107: 509–529.
11. Fischer D W and Baun W L (1968) Band structure and the titanium L II, III X-ray emission and absorption spectra from pure metal, oxides, nitride, carbide, and boride. *J. Appl. Phys.* 39: 4757–4776.
12. Bearden J A (1967) X-ray wavelength. *Rev. Mod. Phys.* 39: 78–124.
13. Augustsson A, Zhuang G V, Butorin S M, Osorio-Guillén J M, Dong C L, Ahuja R, Chang C L, Ross P N, Nordgren J, and Guo J H (2005) Electronic structure of phospho-olivines Li_xFePO_4 (X=0,1) from soft-x-ray-absorption and -emission spectroscopies. *J. Chem. Phys.* 123: 184717.
14. Tompson P, Cox D E, and Hastings J B (1987) Rietveld refinement of Debye-Scherrer synchrotoron X-ray data from Al2O3. *J. Appl. Cryst.* 20: 79–83.

15. Van Aken P A, Liebscher B, and Styrsa V J (1998) Quantitative determination of iron oxidation states in minerals using Fe L 2, 3-edge electron energy-loss near-edge structure spectroscopy. *Phys. Chem. Miner.* 25: 323–327.
16. Van Aken P A and Liebscher B (2002) Quantification of ferrous/ferric ratios in minerals: new evaluation schemes of Fe L 23 electron energy-loss near-edge spectra. *Phys. Chem. Miner.* 29: 188–200.
17. Leapman R D, Grunes L A, and Fejes P L (1982) Study of the L23 edges in the 3d transition metals and their oxides by electron-energy-loss spectroscopy with comparisons to theory. *Phys. Rev. B* 26: 614–635.
18. Mitsunobu S, Ohashi Y, Makita H, Suzuki Y, Nozaki T, Ohigashi T, Ina T, and Takaki Y (2021) One year *in situ* incubation of pyrite at the deep seafloor and its microbiological and biochemical characterizations. *Appl. Environ. Microbiol.* 87.
19. Nakada R, Sato M, Ushioda M, Tamura Y, and Yamamoto S (2019) Variation of iron species in plagioclase crystals by X-ray absorption fine structure analysis. *Geochem. Geophys. Geosystems* 20: 5319–5333.
20. Zhu H, Huang Y, Zhu H, Wang L, Lan S, Xia X, and Liu Q (2020) In situ probing multiple-scale structures of energy materials for Li-ion batteries. *Small Methods* 4: 1900223.